Tandem *in situ* monitoring for quantitative assessment of mechanochemical reactions involving structurally unknown phases

Stipe Lukin, Tomislav Stolar, Martina Tireli, Maria Valeria Blanco, Darko Babić, Tomislav Friščić, Krunoslav Užarević,* and Ivan Halasz*

We report here quantitative in situ monitoring via simultaneous PXRD and Raman spectroscopy of the mechanochemical reaction between benzoic acid and nicotinamide, affording a rich polymorphic system with four new cocrystal polymorphs, multiple phase transformations and a variety of reaction pathways. After observing polymorphs by in situ monitoring, we were able to isolate and characterize three of the four polymorphs, most of which are not accessible from solution. Relative stabilities among the isolated polymorphs at ambient conditions were established by slurry experiments. Using two complementary methods for in situ monitoring enabled quantitative assessment and kinetic analysis of each studied mechanochemical reaction, even when involving unknown crystal structures, and short-lived intermediates. In situ Raman monitoring was introduced here also as a standalone laboratory technique for quantitative assessment of mechanochemical reactions and understanding of mechanochemical reactivity. Our results provide an important step toward a complete and high-throughput quantitative approach to mechanochemical reaction kinetics and mechanisms, necessary for the development of the mechanistic framework of milling reactions.

1 Introduction

Mechanochemical milling is emerging as a versatile synthesis techniques for a variety of chemical transformations,[1,2] including synthesis and screening of cocrystal forms[3–7] and polymorphs.[8–14] Despite the long history of mechanochemistry[15,16] and the use of milling in various branches of chemical and materials processing,[17–20] the underlying mechanistic details of these reactions are only now becoming accessible, enabled by the recent development of *in situ* reaction monitoring techniques based on powder X-ray diffraction (PXRD),[21] Raman spectroscopy[22] and a combination of the two.[23] These advanced techniques have revealed a surprising level of complexity in milling reactions, involving crystalline and amorphous intermediates, as well as multi-step reaction mechanisms that can be sensitive to slight variations in reaction conditions.[24]

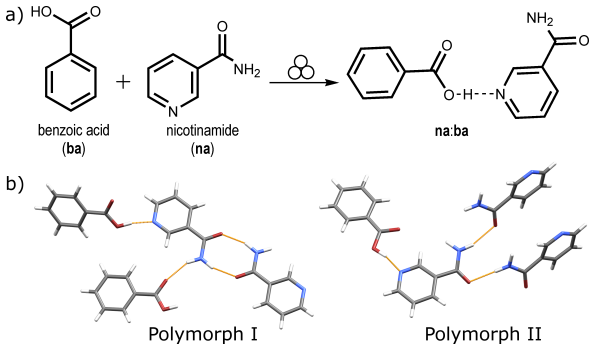

Fig. 1 a) Mechanochemical cocrystallisation of benzoic acid and nicotinamide, and b) hydrogen-bonding in crystal structures of polymorphs **I** and **II**.

While qualitative evaluation of mechanochemical reaction is now generally available, a persistent major challenge in mechanochemical reactions still remains the absence of their mechanistic understanding, primarily resulting from the inability of quantitative evaluation of mechanochemical reaction kinetics. Quantitative *in situ* reaction monitoring has thus far been limited to synchrotron PXRD,[25,26] and only to those systems where crystal structures of all participating phases were known, enabling Rietveld analysis. Consequently, a reaction product or an intermediate with an unknown crystal structure represents an insurmountable problem for quantitative Rietveld analysis as well as addressing the chemical composition of any amorphous phases that can easily be generated during milling.[25,26]

To remedy the currently very scarce mechanistic understanding of mechanochemical milling reactions, accumulation of knowledge of reaction profiles for a large number of reactions and reaction types will be required. While Raman spectroscopy has been used to monitor mechanochemical reactions *in situ* and *ex situ*, current approaches mostly relied on extracting the reaction profile from changes in the intensity of a single peak.[27,28] Clearly, continuing in this fashion would present a tedious task for collecting sufficient kinetic data for a variety of mechanochemical reactions conducted under a variety of reaction conditions. Additionally, *ex situ* approach is not suitable for self-propagating and air-sensitive reactions, as well as the use of volatile additives.[22]

Herein, we describe tandem *in situ* mechanochemical reaction monitoring, with time-resolution in seconds, combined with a

[*] S. Lukin, T. Stolar, M. Tireli, Dr. D. Babić, Prof. T. Friščić, Dr. K. Užarević, Dr. I. Halasz
Ruđer Bošković Institute, Bijenička c. 54, 10000 Zagreb (Croatia)
E-mail: ivan.halasz@irb.hr
krunoslav.uzarevic@irb.hr
Dr. M. V. Blanco,
ESRF - the European Synchrotron, Grenoble (France)
Prof. T. Friščić,
Department of Chemistry, McGill University, Montreal (Canada)
Supporting information for this article is available on the WWW under http://dx.doi.org/10.XXXX/XXXX

high-throughput analysis to extract reaction concentration profiles. Additionally, we were able to use Raman *in situ* monitoring to quantitatively assess reaction profiles even in situations where Rietveld refinement was not possible since not all of the participating phases have been structurally characterized which hindered . Our approach is verified on a challenging model system that involves cocrystallization of pharmaceutically relevant benzoic acid (**ba**) with the model active pharmaceutical ingredient nicotinamide (**na**) in a dynamic reaction environment involving multiple polymorphic transformations, fast kinetics, novel crystalline phases and short-lived intermediates (Scheme 1).

2 Experimental Section

Mechanochemical reactions were carried out by using IST500 (InSolido Technologies, Croatia) or MM301 (Retsch, Germany) mixer mills operating at 30 Hz in translucent and amorphous reaction vessels made from polymethylmetacrylate (PMMA). Two halves of the vessel snapped upon closure to form a leak proof seal. Liquids for liquid-assisted grinding were added using Gilson automated micro pipette.

Tandem *in situ* monitoring experiments were conducted in the experimental hutch of the ESRF air-conditioned to 20 °C. The X-ray beam ($\lambda = 0.195$ Å) and the Raman laser ($\lambda = 785$ nm) focus were positioned to approximately coincide during milling in order to collect data on the same portion of the reaction mixture. X-ray radiation wavelength of 0.195 Å was selected using a multilayer monochromator. Diffraction data were recorded on a Dectris Pilatus CdTe 2M detector positioned 1067 mm from the sample. Radial integration of the raw diffraction images was performed using PyFAI.[29] Exposure time for each pattern was 5 s while time resolution between consecutive patterns was ca. 6.5 s. Time resolution of Raman spectra was typically 10 s.

In situ monitoring was conducted at the new ID31 high-energy beamline of the European Synchrotron Radiation Facility (ESRF) using a ball mill custom modified to allow for simultaneous X-ray diffraction[30] and Raman monitoring.[22] Reactants, 1 mmol (122 mg) of **na** and 1 mmol (122 mg) of **ba** were weighed in separate halves of the reaction vessel to avoid contact before milling. As milling media two 7 mm stainless steel balls were used, each weighing 1.4 g. Each experiment was started with a new, pristine reaction vessel to reduce the risk of possible contamination with crystal seeds from earlier experiments.[31] Tandem *in situ* monitoring was performed on neat grinding as well as on LAG reactions involving as additives water or simple aliphatic alcohols (methanol, ethanol, 1-propanol, 1-butanol) added in the amount of 0.1 mmol.

Where possible, quantitative Rietveld refinement[32] was performed on *in situ* collected powder diffraction patterns. Crystal structures of **III** and **IV** are not known, which limited the use of Rietveld refinement of data sets where they had formed. The first diffraction pattern was sometimes excluded from the analysis due to it still having a non-uniform mixture composition. The Rietveld refinement on a series of patterns was performed in an automated fashion using the command-line version of Topas, usually always starting from the same input file which was prepared so that each phase had its scale factor between its lowest and highest observed values for that milling experiment. In our case, this proved a better approach then sequential refinement, which takes the output of the previous refinement as an input for the next one, which often resulted in meaningless parameter values toward the end of the run. Rietveld refinements included refinement of the parameters for the shifted Chebyshev polynomial used to describe the background parameters, parameters contributing the peak position and shape (contribution to the lorenzian and gaussian full widths at half maximum, zero shift, unit cell parameters). The structure models were taken as solved from powder diffraction data (see section S6). No instrument contribution to the peak shape was assumed. In each cycle of Rietveld refinement, after reaching convergence, weight fractions of refined phase were output to a separate file. All calculations were performed using the program Topas.

Figures showing two-dimensional time-resolved PXRD or Raman data were created using the program Mathematica with the help of the SciDraw package.[33] Background of each diffraction pattern was subtracted prior to plotting using the Sonneveld-Visser[34] algorithm which we have implemented in *Mathematica*.

Laboratory *in situ* Raman monitoring was performed using an IST500 mixer ball mill from InSolido Technologies (Croatia) operating at 30 Hz. Time-resolved *in situ* Raman spectra were collected as described previously.[22] Raman monitoring was performed using a portable Raman system with a PD-LD (now Necsel) BlueBox laser source (excitation wavelength 785 nm) equipped with B&W-Tek fiber optic Raman BAC102 probe, and coupled with OceanOptics Maya2000Pro spectrometer. Probe was positioned under the milling vessel using a movable stand, so to place a focus of the laser 1 mm inside of the vessel. In each experiment, after the monitoring was finished, the sample was taken out and analyzed by PXRD.

Reaction vessel subtraction. Raman spectrum of the PMMA reaction vessel was taken in the same experimental conditions in which all mechanochemical experiments were performed (mill operating at 30 Hz vessel being mounted at the same distance from the probe). For subtracting the vessel contribution from experimental spectra, the peak at 2955 cm^{-1}, corresponding to the C–H bond stretching of PMMA, was used as the reference for scaling. From the *ex situ* analysis it was found that it does not overlap with any peak of reactant and product phases. Spectral range of $2889-3007\,cm^{-1}$ (61 points) was background corrected with Sonneveld-Visser[34] algorithm in both the experimental and the vessel Raman spectra. The intensities of the experimental spectrum in the range $2933-2968\,cm^{-1}$ (19 points) were divided by those of the vessel spectrum. The mean quotient value was used as the scaling factor by which the whole vessel spectrum was multiplied and subtracted from the experimental one. This procedure was repeated for all experimental spectra to provide pure spectra without the vessel contribution.

Analysis of Raman spectra. For acquisition of the Raman spectra of pure **na** and **ba**, 2 mmol of each was grinded separately in the same experimental conditions. Average spectrum

was taken as the pure spectrum for each of these two phases. The spectra of pure **I**, **II** and **III** were taken from the in situ experiments, from the parts of the reaction where PXRD showed that they were present as a pure phase. All spectra were baseline corrected using asymmetric least squares smoothing[35] (AsLS) method.

Phase **IV** could be observed as fleeting intermediate in LAG reactions with alcohols. Since it could not be isolated as a pure phase, its Raman spectrum could not be obtained as for **I**, **II** and **III**. Multivariate curve resolution - alternating least squares[36] (MCR-ALS) was performed on the data from LAG reactions with ethanol, 1 propanol and 1 butanol in an attempt to estimate the Raman spectrum of **IV**. Non-negativity was enforced to both mole fraction and spectral profiles. Additionally, sum of the mole fractions was required to be 1. Prior to the analysis all spectra were normalized. The obtained spectrum of **IV** was very similar to **III**, which also agreed well with the findings from PXRD analysis. However, when other experimental spectra were analyzed with this spectrum included, there were obvious artifacts in the mole fraction profiles. Actually, it was found that by using the spectrum of **III** instead of **IV**, more sensible results are obtained, although it looks clear that the transient intermediate **IV** can not be **III**.

Reaction evolution profiles were analyzed by using the restrained classical least squares method implemented in MCR-ALS GUI[37], including the closure and non-negativity constraints together with an equality constraint for the spectra of pure phases. Prior to the analysis all experimental spectra and the spectra of pure phases were normalized. Standard deviations for mole fractions estimated from the k-th experimental spectrum were computed from the covariance matrix:

$$\mathbf{Cov} = \sigma^2(\mathbf{S}\mathbf{S}^{\mathrm{T}})^{-1}$$

where $\mathbf{S}$ is the matrix with row-wise spectra of pure components and σ^2 is the variance of the residuals for the k-th experimental spectrum

$$\sigma^2 = \frac{\mathbf{e}^{\mathbf{T}}\mathbf{e}}{n-p}$$

and $\mathbf{e}$ is the vector of residuals, n is the number of spectrum points and p is the number of estimated regression coefficients (mole fractions).

This approach gave very good quantitative results for evolution of reaction mixture that agreed well with the quantitative Rietveld analysis of PXRD data. Example quantitative Raman analysis is given in Section S4 in Figs. S9–S20.

Laboratory powder X-ray diffraction (PXRD) patterns were collected using a Philips PW 3710 diffractometer with a CuKα radiation, tension 40kV, and current 40 mA, with a flat plate sample on a zero background in Bragg-Brentano geometry. The patterns were collected in the 2θ range of 4° to 40° with a step size of 0.02° and 1.0 s counting per step.

Thermal analysis. Differential scanning calorimetry (DSC) experiments were performed on Discovery DSC (TA Instruments). Around 2 mg of each sample was put in aluminum crucible. All samples were measured in the range of 25 °C to 400 °C with a heating rate of 5.0 °C/ min. Experiments were performed in an inert N_2 atmosphere. Thermal stability of **na**:**ba** cocrystal polymorphs were determined from TGA experiments (Discovery TGA, TA Instruments). Around 5 mg to 10 mg of each sample was put in platinum HT pan type. All samples were heated at the rate of 5.0 °C/ min up to 400 °C. Experiments were performed in an inert N_2 atmosphere.

Fourier-transform infrared attenuated total reflectance (FTIR-ATR) measurements were performed on a Perkin-Elmer Spectrum Two instrument equipped with a diamond crystal Quest ATR Accessory. The measurements were taken in the range of 4000–400 cm^{-1}.

3 Results and discussion

Although **na** and **ba** are ubiquitous molecules which have complementary hydrogen-bonding functionalities, and have been widely investigated as components of cocrystals,[38–47] their mutual cocrystallization has not yet been described. The herein conducted mechanochemical reactions of the 1:1 stoichiometric mixture of solid **na** and **ba**, either by liquid-assisted grinding (LAG)[12,48] or by neat grinding (NG), led us to discover four new crystalline phases in this cocrystal system. The phases **I** and **II** were structurally characterized as polymorphs of the 1:1 **na**:**ba** cocrystal while crystal structures of phases **III** and **IV** currently remain unknown. The crystal structures of both **I** and **II** were solved from PXRD data collected on the mechanochemically prepared samples (Section S6 in the Supporting Information). In both polymorphs the −COOH group of **ba** forms a hydrogen bond towards the pyridine nitrogen of **na**. Whereas in **I** two molecules of **na** associate through hydrogen bonds to form dimers, in **II** the **na** molecules are assembled into an extended hydrogen-bonded network (Scheme 1b).

Our attempts to solve the crystal structure of **III** from PXRD data have been unsuccessful, as were attempts to grow single crystals of **III** from solution (Section S7). PXRD analysis however, shows that **III** is obtained as a pure phase starting from the 1:1 **na**:**ba** mixture. Spectroscopic (Figs. S37, S38) and thermal analyses (Fig. S41) are consistent with **III** being a 1:1 cocrystal of **na** and **ba** and, therefore, a polymorph of **I** and **II**. In contrast, the phase **IV** was observed only during *in situ* monitoring experiments and was never obtained as a pure phase.

Tandem *in situ* monitoring was conducted at the new ID31 high-energy beamline of the European Synchrotron Radiation Facility (ESRF) using a mixer ball mill custom modified to allow for tandem X-ray diffraction[30] and Raman monitoring.[22] Reactions were conducted in amorphous and transparent polymethylmetacrylate reaction vessels oscillated at 30 Hz in a horizontal plane. The X-ray beam was passed through the bottom of the reaction vessel while the incident laser for Raman spectroscopy was set to enter the vessel from below and to coincide with the X-ray beam. Reactants, 1 mmol (122 mg) of **na** and 1 mmol (also 122 mg) of **ba**, were weighed in separate halves of the reaction vessel to avoid contact before milling. As milling media two 7 mm stain-

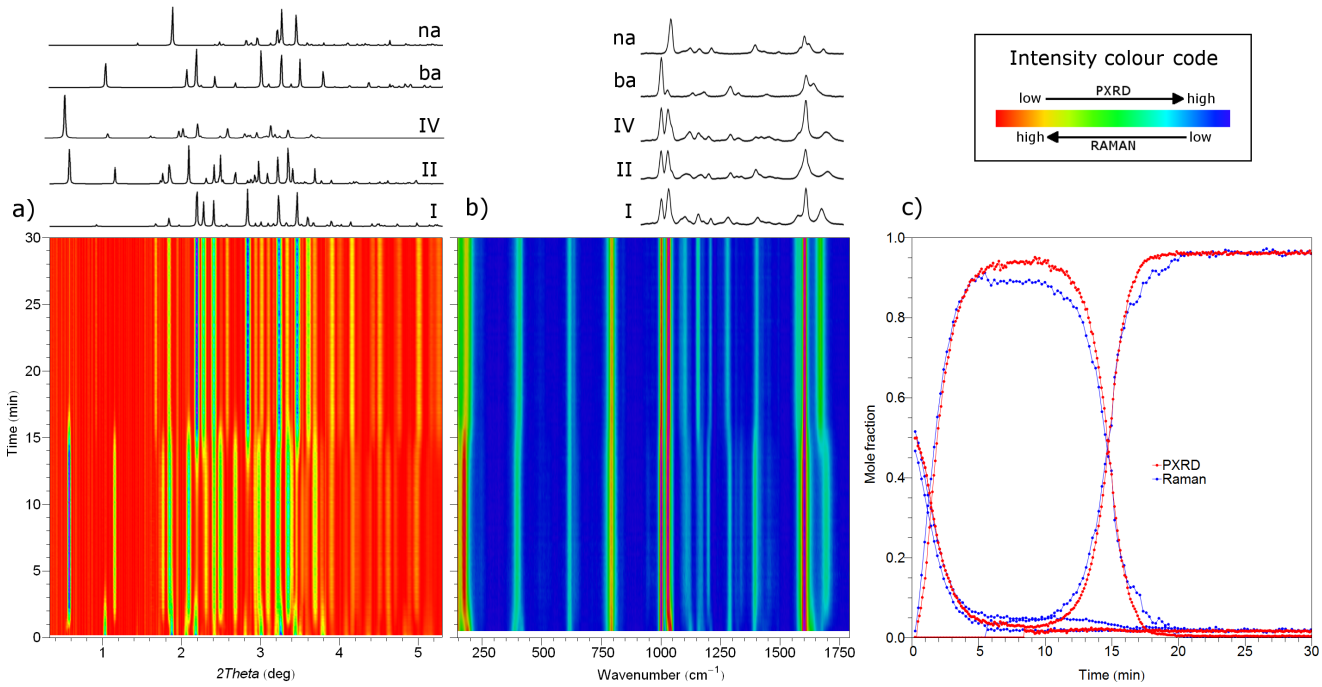

Fig. 2 Tandem *in situ* monitoring by (a) PXRD and (b) Raman spectroscopy of the LAG reaction of the 1:1 **na**:**ba** mixture using water. PXRD patterns and Raman spectra of pure components are given on top. The shown portion of Raman spectra was used in quantitative analysis. (c) Comparison of the evolution of the reaction mixture composition derived from time-resolved PXRD patterns and Raman spectra.

less steel balls were used, each weighing 1.4 g. Each experiment was started with a new, pristine reaction vessel to reduce the risk of possible contamination with crystal seeds from earlier experiments.[31] LAG reactions included 0.1 mmol (10 mol% relative to the **na**:**ba** mixture) of water or simple aliphatic alcohols as liquid additives.

3.1 Qualitative analysis

A LAG reaction using water (2.0 μL) as the liquid additive yielded a stepwise reaction with polymorph **I** as the final product which formed from polymorph **II** ca. 15 min into milling (Figs. 2, S6). The formation of **II** was here preceded by the appearance of a tiny amount of **IV**. Replacing water with methanol (MeOH, 4.1 μL) led to an immediate formation of the short-lived phase **IV**, followed by the formation of **II** (Figs. 3a, S7). The reaction was complete within ca. 6 min, and polymorph **II** was stable upon further grinding (Fig. S2). In repeated experiments, polymorph **II** was stable even up to 3 h milling. The LAG reaction using ethanol (EtOH, 6.2 μL) also began with immediate formation of **IV**, which persisted for up to ca. 2 min of milling (Fig. S3). It was followed by phase **II**, which transformed into **I** after ca. 10 min milling. LAG reactions involving 1-propanol (1-PrOH, 7.5 μL) (Fig. S4) or 1-butanol (1-BuOH, 9.2 μL) both led to **III** as the final product. These two reactions also proceeded *via* rapid formation of phase **IV**, followed by phase **II** which, ultimately, over a period of ca. 10-20 minutes, transformed to phase **III** (Fig. 4).

Finally, we have performed tandem *in situ* monitoring under neat grinding conditions. Similar to LAG with water and EtOH, NG after 60 min milling also yielded **I** as the final pure product (Figs. 5, S8). However, *in situ* monitoring revealed a significantly slower, stepwise reaction where the phase **III** was formed initially, and transformed into phase **I** after ca. 20 min milling.

3.2 Polymorph stability

Slurry experiments revealed that **I** is the thermodynamically stable form of the **na**:**ba** cocrystal at ambient conditions, followed by phases **III** and **II** in decreasing order of stability. Based on its fast formation and fleeting existence, we surmise that **IV** is the least stable among the four herein reported phases. The observed mechanochemical reaction pathways exhibit stepwise reaction mechanism that lead to increasingly stable phases in consistence with the Ostwald's rule of stages.[49] Once isolated, phases **I**, **II** and **III** were stable for months.

3.3 Quantitative assessment and kinetic analysis

While tandem PXRD and Raman *in situ* monitoring experiments are readily compared by plotting on the same time scale, quantitative assessment not only provides detailed insight to species involved in the reaction but also permits its kinetic modeling. Quantitative assessment by PXRD monitoring was possible only in systems where crystal structures of all participating phases were known enabling Rietveld refinement, in a similar manner as described previously.[6,21,26,50] Example Rietveld refinement plots are given in Supporting Information section S3. On the other hand, quantitative assessment via Raman monitoring is more versatile, particularly if participating phases can be isolated as pure phases.

In kinetic assessment, one caveat should be kept in mind. Namely, the reaction mixture is warming up during milling[28,51] which could influence reaction kinetics as the reaction is oc-

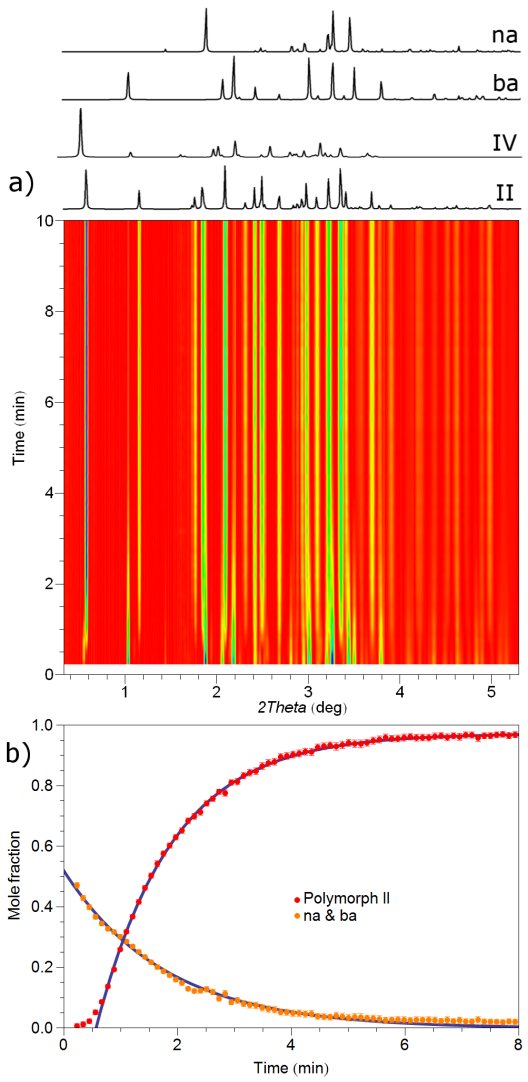

Fig. 3 (a) First 10 min of *in situ* PXRD monitoring of a LAG reaction using 0.1 mmol (4.1 μL) of methanol. Intermediate **IV** can be observed in the first minute of milling. Calculated diffraction patterns are displayed on top. (b) Reaction profile derived from Rietveld refinement. Both curves fit the first-order reaction rate.

curring. Recently, we have shown that even mild temperature changes, achieved by preheating the milling assembly, can a have a dramatic influence on reaction kinetics and mechanism.[26] Here, all the reactions were conducted under the same reaction conditions which allows us the possibility to compare different reactions, even though the reaction kinetics in each individual reaction may have been changing during milling.

The Raman spectra were analyzed by using the spectra of reactant components and of the recognized polymorphic species **I**, **II** and **III**, all recorded under the actual experimental conditions. Most of the spectra were successfully and completely resolved by using invariable spectral components and only reactions involving **IV** remained partially resolved. The concentration profiles obtained from time-resolved Raman spectra are in very good agreement with those obtained by Rietveld analysis of PXRD data (Fig. 2c). Taking into account that Raman spectra of polymorphs **I**, **II** and **III** are sufficiently different, this indicates that under the present experimental conditions, cocrystal formation and polymorphic transformations do not involve a detectable amount of an amorphous phase. High crystallinity is also reflected in stable diffraction peak shape as milling progresses. In general however, a discrepancy in quantitative assessments via PXRD and Raman monitoring could be expected since PXRD is sensitive to bulk crystalline phases while Raman spectroscopy is collecting the scattering signal from all of the sample. In such cases, Raman monitoring could be more informative of mechanochemical reaction mechanism then PXRD since many reactions have a significant amorphous component.[25,26]

For phases that cannot be obtained pure and stable, as was the case here for phase **IV**, we used multivariate curve resolution - alternating least squares[36] (MCR-ALS) to estimate the spectrum of **IV**. However, the estimated spectrum of phase **IV** was strikingly similar to the spectrum of **III** leading to strong correlations between the two in a restrained classic least-squares approach to derive reaction profiles. To avoid correlations between **III** and **IV**, we have used the spectrum of **III** to model also the reaction profile of **IV**. The similarity between spectra of **III** and **IV**, as well as the similarity between PXRD patterns of **III** and **IV**, indicates that these two phases have very similar crystal structures.

Quantitative reaction profiles allowed us to apply solid-state kinetic models[52] in order to describe the mechanistic background of these reactions. Application of these models to mechanochemical milling reaction is not straightforward since these kinetic models were derived primarily for static solid reaction mixtures in contrast to reaction mixtures where particles are undergoing constant breaking and recrystallization as well as stirring by the milling media.[27] At this point, it is safer to avoid kinetic models that stipulate strong assumptions, as for example the popular KJMA kinetic model[53,54] (also known as the Avrami, Avrami-Erofe'ev, JMAEK or Johnson-Mehl model), but rather to use simpler order-based kinetic models[52] or the Prout-Tompkins equation.[55,56]

Focusing first on the depletion of reactants **na** and **ba**, we find it in all LAG reaction (Fig. 6) as well as in NG to be best described by a first-order reaction rate law given by the equation:

$$x = x_\infty + (x_0 - x_\infty)\mathrm{e}^{-k(t-t_0)}$$

where x, x_∞ and x_0 represent average mole fractions of **na** and **ba** at times t, ∞ and t_0, respectively. Constant k is the reaction rate constant and t_0 accounts for the possible time delay from the initiation of milling. Ideally, $x_0 = 0.5$, $x_\infty = 0$, and $t_0 = 0$ but we have allowed a discrepancy from these values to account for the time required for the reaction mixture to become homogeneous.

The LAG reaction using water allows us to compare kinetic modeling on both PXRD and Raman monitoring (Fig. 7). The depletion profiles derived from both techniques led to almost identical first-order reaction rate constants (Table 1) confirming the correspondence between quantitative assessments derived from *in situ* Raman and PXRD monitoring. Rates of reactant consumption are considerably faster in LAG reactions as compared to NG (Table 1, Fig. S5), consistent with the well-known accelerating ef-

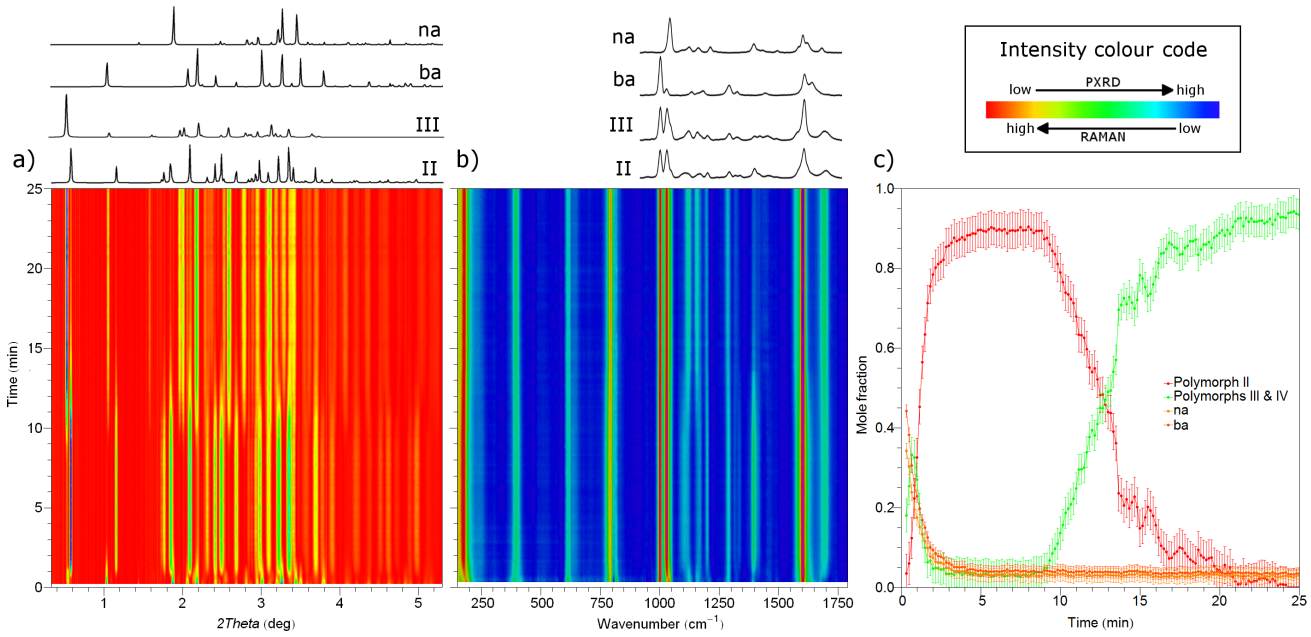

Fig. 4 Tandem *in situ* monitoring by (a) PXRD and (b) Raman spectroscopy of a LAG of 1:1 **na**:**ba** using 10 mol% of 1-butanol. Diffraction patterns and Raman spectra of pure phases are given on top of time-resolved figures. The shown portion of Raman spectra was used in quantitative analysis. c) Evolution of the reaction mixture composition derived from time-resolved Raman spectra in b). Error bars correspond to twice the standard deviations as obtained from the refinement procedure.

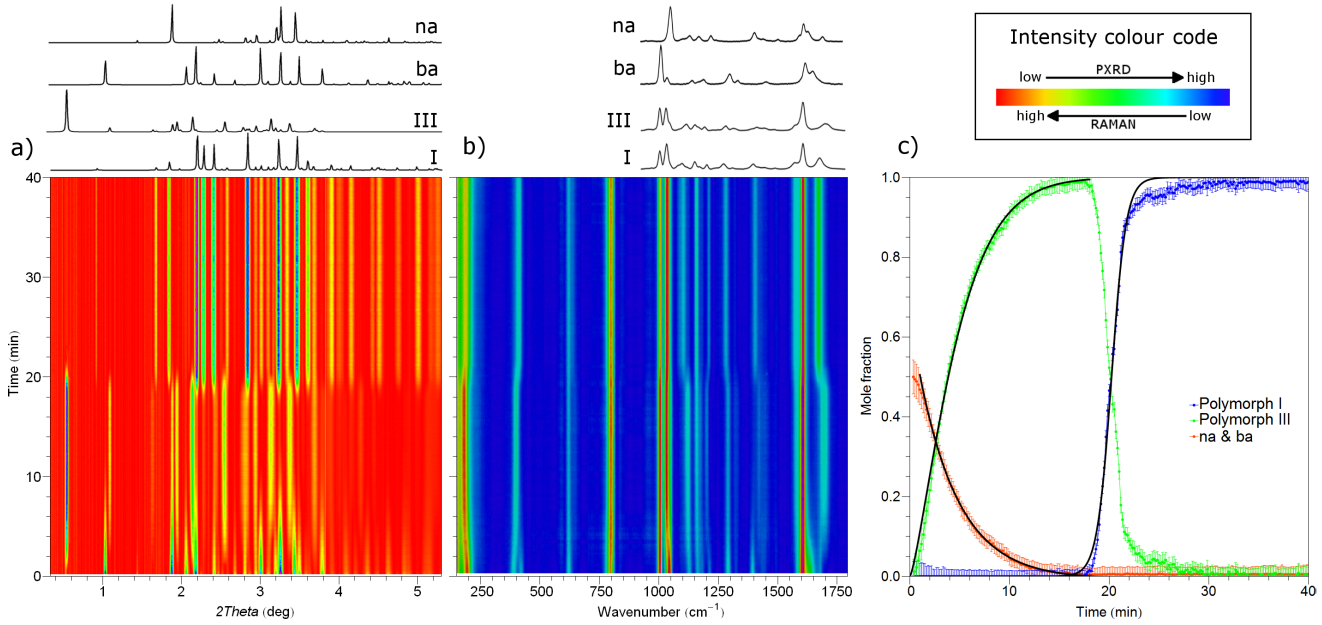

Fig. 5 Tandem *in situ* monitoring by (a) PXRD and (b) Raman spectroscopy of NG of 1:1 **na**:**ba** mixture. Diffraction patterns and Raman spectra of pure phases are given on top of time-resolved figures. The shown portion of Raman spectra was used in quantitative analysis. c) Evolution of the reaction mixture composition derived from time-resolved Raman spectra in b). The fitted curves are displayed in black. Reactant depletion and formation of **III** are described with a first-order reaction rate and the final **III** $\longrightarrow$ **I** transformation with the PT model. Error bars correspond to twice the standard deviations as obtained from the refinement procedure.

fect of liquid additives on mechanochemical reactivity.[6,21,48] The alcohols (added in the amount of 10 mol%) show a constant increase in reaction rate constants while LAG with water seems to be slightly faster then LAG with MeOH.

Formation of **II** in the LAG reaction with water can be well fitted with the first-order reaction rate, the same as for reactant depletion. The subsequent **II** $\longrightarrow$ **I** transformation exhibits a symmetrical and sharp sigmoidal curve that is well described by the Prout-Tompkins (PT) model[55] which assumes a reaction rate proportional to both the amount of the remaining reactant (in this case the mole fraction of phase **II**, $x_{\mathbf{II}}$) and the amount of the already formed product (mole fraction of phase **I**, $x_{\mathbf{I}}$). Assuming

Table 1 Reaction rate constants for the first-order depletion of **na** and **ba** derived from *in situ* Raman monitoring (unless stated otherwise).

	Liquid (10 mol%)					
	NG	water	MeOH	EtOH	1-PrOH	1-BuOH
k/min^{-1}	0.249(2)	0.69(2), 0.68(1)[a]	0.60(1)	0.68(2)	0.82(2)	1.17(1)

[a] From *in situ* PXRD monitoring.

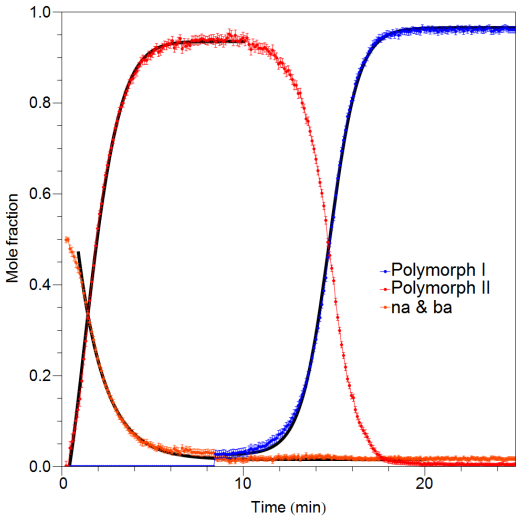

Fig. 6 Fitting the concentration profiles obtained from time-resolved PXRD monitoring for the LAG reaction using water. Depletion of reactants and formation of **II** is described by the first-order reaction rate while the formation of **I** is described by the Prout-Tompkins model. Fitted curves are shown with black lines. Error bars correspond to one standard deviation as obtained from the Rietveld refinement procedure.

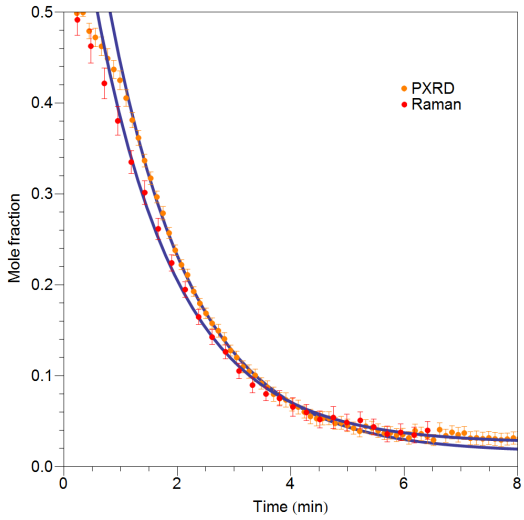

Fig. 7 Comparison of the first-order kinetic modeling of reaction profiles derived from PXRD and Raman monitoring for the LAG reaction using water. The corresponding reaction-rate constants are given in Table 1.

$x_{\mathbf{I}} = 1 - x_{\mathbf{II}}$ we get:

$$\frac{\mathrm{d}x_{\mathbf{I}}}{\mathrm{d}t} = k x_{\mathbf{I}} x_{\mathbf{II}} = k x_{\mathbf{I}} (1 - x_{\mathbf{I}}).$$

For the NG reaction, formation of **III** follows the same first-order reaction rate as the depletion of reactants. The transformation of **III** to **I** commences not before all of **na** and **ba** have completely reacted (Fig. 5c) and exhibits a symmetrical sigmoidal curve that fits best the Prout-Tompkins kinetic model. For NG however, the PT model could not describe that well the initially sharp formation of **I** and slowing down of the reaction toward the end.

The formation of **I** from either **II** or **III** is an autocatalytic nucleation-and-growth process, as indicated by symmetrical sigmoidal growth curves describing the formation of **I**. On the other hand, the rate of **II** $\longrightarrow$ **III** transformation seems to be constant corresponding to a zeroth-order reaction rate law (Figs. 4c, S4). This transformation was notably slower then others and the coexistence of the two phases could be observed even for 20 min (Fig. 4).

3.4 The effect of liquid additive on polymorph selectivity

The formation of phase **IV** seems to be kinetically favored in the presence of alcohols and water as milling additives in all LAG reactions. It is formed immediately upon milling but is soon followed by the formation of polymorph **II**. Stability of polymorph **II** is dependent on LAG conditions employed, where it can remain stable upon further milling or it can convert to either **I** or **III**. In LAG reactions, higher alcohols stabilised **III** while methanol stabilised **II**. However, the increase in molecular weight on going from methanol to 1-butanol increased the ratio of the added liquid volume to the mass of solid reactants, *i. e.* the η-value.[57] Inspired by the recent report from the Jones group, where considerable control over cocrystal polymorphism was achieved simply by changing η,[13] we decided to investigate whether the herein observed reactivity was due to specific interactions between the liquid additive and crystalline particles[11,58] or was it related to the volume of the added liquid.

Therefore, we have conducted laboratory *in situ* Raman monitoring experiments in which the η-value was changed by varying the added liquid volumes. With 9.2 μL, which is the volume originally used for 1-BuOH, and 20 μL, other lower alcohols and also water gave **III** as the final product (Table 2). However, an increased preference for **I** and **II** was observed when using smaller

Table 2 Reaction paths and polymorph selectivity in the mechanochemical 1:1 **na**:**ba** cocrystal formation.

	Volume (μL)		
Liquid	4.1	9.2	20
H_2O	**II**[a]	**II**[a] $\longrightarrow$ **III**	**II**[a] $\longrightarrow$ **III**
MeOH	**IV** $\longrightarrow$ **II**	**II**[a] $\longrightarrow$ **III**	**II**[a] $\longrightarrow$ **III**
EtOH	**II**[a] $\longrightarrow$ **I**	**IV** $\longrightarrow$ **II** $\longrightarrow$ **III**	**IV** $\longrightarrow$ **II** $\longrightarrow$ **III**
PrOH	**II**[a] $\longrightarrow$ **I**	**IV** $\longrightarrow$ **II** $\longrightarrow$ **III**	**IV** $\longrightarrow$ **II** $\longrightarrow$ **III**
BuOH	**II**[a] $\longrightarrow$ **I**	**IV** $\longrightarrow$ **II** $\longrightarrow$ **III**	**IV** $\longrightarrow$ **II** $\longrightarrow$ **III**
Hexane	**III** $\longrightarrow$ **I**	**III** $\longrightarrow$ **I**	**III** $\longrightarrow$ **I**
CH_3CN	**I**	**II** $\longrightarrow$ **I**	**IV** $\longrightarrow$ **II** $\longrightarrow$ **I**

[a] Formation of **IV** before **II** is likely but could not be ascertained from *in situ* Raman monitoring.

volumes. For example, using 4.1 μL of either 1-BuOH, 1-PrOH or EtOH resulted in the formation of **I**. On the other hand, LAG with 4.1 μL of water resulted in the formation of **II**, analogous to what was seen with the same volume of MeOH.

To better understand the role of the hydroxyl group, we have performed laboratory Raman monitoring experiments of LAG reactions using hexane as a pure aliphatic hydrocarbon liquid. Using up to 20 μL of hexane, we observed the same reaction pathway as in NG, yielding initially **III** and finally **I** (Table 2, Fig. S21). Phase **III** was stable in both NG and LAG with hexane while **na** and **ba** were present after which the **III** $\longrightarrow$ **I** transformation began immediately. This suggested surface nucleation of **I** which was prevented during growth of phase **III**.

We have finally performed *in situ* monitoring using acetonitrile as a polar, but aprotic liquid. Acetonitrile could disrupt hydrogen bonds in **ba** and **na** but possibly to a lesser extent then alcohols since it can serve only as a hydrogen-bond acceptor. Indeed, with acetonitrile we have observed a new reaction pathway which depended on the added volume but the final product was always **I**. With 4.1 μL of CH_3CN we have observed direct formation of **I** from **na** and **ba** (Fig. 8). With 9.2 μL, intermediate **II** was formed directly from reactants and transformed later on to **I**. Finally, using 20 μL of CH_3CN, the intermediate **II** was preceded by phase **IV** before the final formation of **I**. Thus, the hydroxyl group is not necessary for the formation of **IV** and other liquids with hydrogen-bonding capabilities can also catalyze its formation. On the other hand, the hydroxyl moiety seems crucial for the stabilization of **III**.

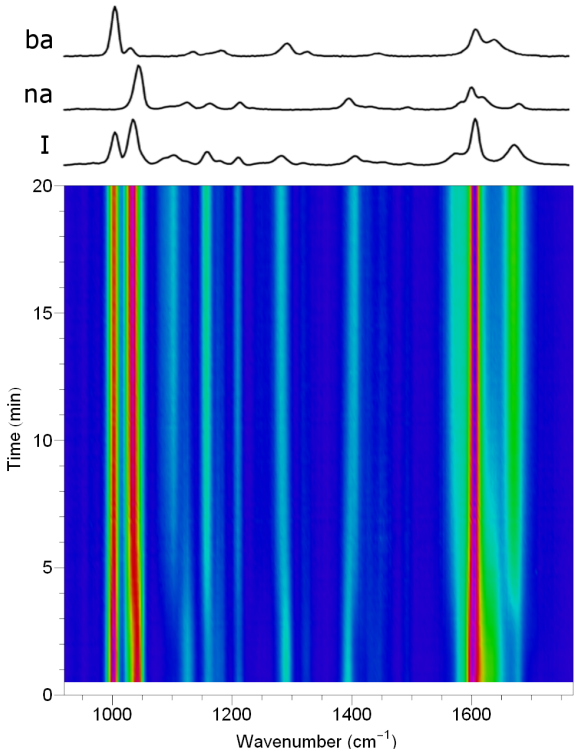

Fig. 8 Raman *in situ* monitoring of 1:1 **na**:**ba** LAG cocrystallization using 4 μL of acetonitrile as the liquid additive. The reaction yields directly polymorph **I** as the final product.

4 Conclusion

In summary, tandem *in situ* monitoring *via* PXRD and Raman spectroscopy of the mechanochemical cocrystallisation of **na** and **ba** revealed a rich polymorphic system with four new cocrystal phases, multiple phase transformations and a variety of reaction pathways that can be controlled by a careful choice of reaction conditions. The reaction pathway and selectivity can be altered and controlled by the type of the liquid additive in LAG reactions as well as by its amount. The reaction kinetics were quantitatively assessed from tandem *in situ* monitoring, performed in seconds-time resolution, even in situations where not all crystalline phases were structurally characterized. We found reactant depletion to be well described by the first order reaction rate law kinetics while product formation was usually an autocatalytic process.

We also introduce here quantitative *in situ* Raman monitoring as a technique that is readily implemented in a conventional laboratory as opposed to PXRD monitoring that can be performed only at dedicated synchrotron beamlines. In systems where the reaction mixture is highly crystalline, quantification via PXRD or Raman monitoring will provide similar results but we anticipate that quantitative Raman monitoring could be used to characterize amorphous phases which are known to occur during milling of pharmaceutical materials[6,59] and in solid-state reactions in general. Our results provide an important first step toward complete quantification of mechanochemical reaction kinetics and emphasize *in situ* monitoring as necessary analytical tools for understanding of mechanochemical reactivity. The ability to describe reaction kinetics by the simple order-based and Prout-Tompkins reaction models hints the possibility that mechanochemical reactions may bear stronger similarities to solution reactions than could be expected for reactions of solids. By establishing these procedures as a standard in mechanochemical synthesis, we anticipate they will provide the basis for the development of kinetic models of milling reactions and enable formulation of a general mechanistic framework of these increasingly important reactions.

Acknowledgements

We are grateful to Mr. Vitomir Stanišić, Mr. Ivan Kulcsár and their team at the Ruđer Bošković Institute for continuous support and Mr. Hrvoje Dagelić for programming. Dr. Dejan-Krešimir Bučar, Dr. Dubravka Šišak and Dr. Manda Ćurić are acknowledged for critically reading the manuscript. Financial support from the ESRF and the Croatian Science Foundation (Grant No. UIP–2014–09–4744) is gratefully acknowledged. IH is grateful to the Adris foundation for supporting this work. SL is supported by the Croatian Science Foundation. TF acknowledges the financial support of the NSERC Discovery Grant and the McGill University W. J. Dawson Scholarship.

References

1 S. L. James, C. J. Adams, C. Bolm, D. Braga, P. Collier, T. Friščić, F. Grepioni, K. D. M. Harris, G. Hyett, W. Jones, A. Krebs, J. Mack, L. Maini, A. G. Orpen, I. P. Parkin, W. C. Shearouse, J. W. Steed, D. C. Waddell, *Chem. Soc. Rev.* **2012**, *41*, 413–447.

2 J. G. Hernandez, C. Bolm, *J. Org. Chem.* **2017**, *82*, 4007–4019.

3 D. Braga, L. Maini, F. Grepioni, *Chem. Soc. Rev.* **2013**, *42*, 7638–7648.

4 T. Friščić, W. Jones, *Cryst. Growth Des.* **2009**, *9*, 1621–1637.

5 C. Aakeröy, *Acta Cryst.* **2015**, *B71*, 387–391.

6 I. Halasz, A. Puškarić, S. A. J. Kimber, P. J. Beldon, A. M. Belenguer, F. Adams, V. Honkimäki, R. E. Dinnebier, B. Patel, W. Jones, V. Štrukil, T. Friščić, *Angew. Chem. Int. Ed.* **2013**, *52*, 11538–11541.

7 M. K. Corpinot, S. A. Stratford, M. Arhangelskis, J. Anka-Lufford, I. Halasz, N. Judaš, W. Jones, D.-K. Bučar, *CrystEngComm* **2016**, *18*, 5434–5439.

8 S. Aitipamula, P. Chow, R. Tan, *CrystEngComm* **2014**, *16*, 3451–3465.

9 E. Losev, E. Boldyreva, *CrystEngComm* **2014**, *16*, 3857–3866.

10 F. Fischer, G. Scholz, S. Benemann, K. Rademann, F. Emmerling, *CrystEngComm* **2014**, *16*, 8272–8278.

11 A. M. Belenguer, G. I. Lampronti, A. J. Cruz-Cabeza, C. A. Hunter, J. K. M. Sanders, *Chem. Sci.* **2016**, *7*, 6617–6627.

12 A. V. Trask, N. Shan, W. D. S. Motherwell, W. Jones, S. Feng, R. B. H. Tan, K. J. Carpenter, *Chem. Commun.* **2005**, 880–882.

13 D. Hasa, E. Miniussi, W. Jones, *Cryst. Growth Des.* **2016**, *16*, 4582–4588.

14 F. Fischer, A. Heidrich, S. Greiser, S. Benemann, K. Rademann, F. Emmerling, *Cryst. Growth Des.* **2016**, *16*, 1701–1707.

15 L. Takacs, *Chem. Soc. Rev.* **2013**, *42*, 7649–7659.

16 E. Boldyreva, *Chem. Soc. Rev.* **2013**, *42*, 7719–7738.

17 A. D. Jodlowski, A. Yépez, R. Luque, L. Camacho, G. de Miguel, *Angew. Chem. Int. Ed.* **2016**, *55*, 14972–14977.

18 P. Baláž, M. Achimovičová, M. Baláž, P. Billik, Z. Cherkezova-Zheleva, J. M. Criado, F. Delogu, E. Dutková, E. Gaffet, F. J. Gotor, R. Kumar, I. Mitov, T. Rojac, M. Senna, A. Streletskii, K. Wieczorek-Ciurowa, *Chem. Soc. Rev.* **2013**, *42*, 7571–7637.

19 G.-W. Wang, *Chem. Soc. Rev.* **2013**, *42*, 7668–7700.

20 K. Užarević, I. Halasz, I. Đilović, N. Bregović, M. Rubčić, D. Matković-Čalogović, V. Tomišić, *Angew. Chem. Int. Ed.* **2013**, *52*, 5504–5508.

21 T. Friščić, I. Halasz, P. A. Beldon, A. M. Belenguer, F. Adams, S. A. J. Kimber, V. Honkimäki, R. E. Dinnebier, *Nature Chem.* **2013**, *5*, 66–73.

22 D. Gracin, V. Štrukil, T. Friščić, I. Halasz, K. Užarević, *Angew. Chem. Int. Ed.* **2014**, *53*, 6193–6197.

23 L. Batzdorf, F. Fischer, M. Wilke, K.-J. r. Wenzel, F. Emmerling, *Angew. Chem. Int. Ed.* **2015**, *54*, 1799–1802.

24 K. Užarević, I. Halasz, T. Friščić, *J. Phys. Chem. Lett.* **2015**, *6*, 4129–4140.

25 I. Halasz, T. Friščić, S. A. J. Kimber, K. Užarević, A. Puškarić, C. Mottillo, P. Julien, V. Štrukil, V. Honkimäki, R. E. Dinnebier, *Faraday Discuss.* **2014**, *170*, 203–221.

26 K. Užarević, V. Štrukil, C. Mottillo, P. A. Julien, A. Puškarić, T. Friščić, I. Halasz, *Cryst. Growth Des.* **2016**, *16*, 2342–2347.

27 X. Ma, W. Yuan, S. E. J. Bell, S. L. James, *Chem. Commun.* **2014**, *50*, 1585–1587.

28 F. Fischer, K.-J. Wenzel, K. Rademann, F. Emmerling, *Phys. Chem. Chem. Phys.* **2016**, *18*, 23320–23325.

29 J. Kieffer, D. Karkoulis, *Journal of Physics: Conference Series* **2013**, *425*, 202012.

30 I. Halasz, S. A. J. Kimber, P. J. Beldon, A. M. Belenguer, F. Adams, V. Honkimäki, R. C. Nightingale, R. E. Dinnebier, T. Friščić, *Nat. Protoc.* **2013**, *8*, 1718–1729.

31 D.-K. Bučar, G. M. Day, I. Halasz, G. G. Z. Zhang, J. R. G. Sander, D. G. Reid, L. R. MacGillivray, M. J. Duer, W. Jones, *Chem. Sci.* **2013**, *4*, 4417–4425.

32 R. J. Hill, C. J. Howard, *J. Appl.Cryst.* **1987**, *20*, 467–474.

33 M. Caprio, *Comput. Phys. Commun.* **2005**, *171*, 107 – 118.

34 E. J. Sonneveld, J. W. Visser, *J. Appl. Cryst.* **1975**, *8*, 1–7.

35 P. H. C. Eilers, H. F. M. Boelens, *Leiden University Medical Center Report* **2005**.

36 A. de Juan, J. Jaumot, R. Tauler, *Anal. Methods* **2014**, *6*, 4964–4976.

37 J. Jaumot, A. de Juan, R. Tauler, *Chemometr. Intell. Lab.* **2015**, *140*, 1 – 12.

38 N. Schultheiss, A. Newman, *Cryst. Growth Des.* **2009**, *9*, 2950–2967.

39 S. Aitipamula, A. Wong, P. Chow, R. Tan, *CrystEngComm* **2012**, *14*, 8193–8198.

40 S. G. Fleischman, S. S. Kuduva, J. A. McMahon, B. Moulton, R. D. Bailey Walsh, N. Rodriguez-Hornedo, M. J. Zaworotko, *Cryst. Growth Des.* **2003**, *3*, 909–919.

41 D. J. Berry, C. C. Seaton, W. Clegg, R. W. Harrington, S. J. Coles, P. N. Horton, M. B. Hursthouse, R. Storey, W. Jones, T. Friščić, N. Blagden, *Cryst. Growth Des.* **2008**, *8*, 1697–1712.

42 S. Karki, T. Friščić, W. Jones, *CrystEngComm* **2009**, *11*, 470–481.

43 F. Fischer, D. Lubjuhn, S. Greiser, K. Rademann, F. Emmerling, *Cryst. Growth Des.* **2016**, *16*, 5843–5851.

44 R. Dubey, G. R. Desiraju, *Chem. Commun.* **2014**, *50*, 1181–1184.

45 C. C. Seaton, A. Parkin, C. C. Wilson, N. Blagden, *Cryst. Growth Des.* **2009**, *9*, 47–56.

46 H. C. S. Chan, J. Kendrick, M. A. Neumann, F. J. J. Leusen, *CrystEngComm* **2013**, *15*, 3799–3807.

47 N. Chieng, M. Hubert, D. Saville, T. Rades, J. Aaltonen, *Cryst. Growth Des.* **2009**, *9*, 2377–2386.

48 N. Shan, F. Toda, W. Jones, *Chem. Commun.* **2002**, 2372–2373.

49 J. C. Burley, M. J. Duer, R. S. Stein, R. M. Vrcelj, *Eur. J. Pharm. Sci.* **2007**, *31*, 271 – 276.

50 A. D. Katsenis, P. A., V. Štrukil, C. Mottillo, P. A. Julien, M. H. Užarević, K. Pham, T. O. Do, S. A. J. Kimber, P. Lazić, O. Magdysyuk, R. E. Dinnebier, I. Halasz, T. Friščić, *Nat. Commun.* **2015**, *6*, 6662.

51 H. Kulla, M. Wilke, F. Fischer, M. Rollig, C. Maierhofer, F. Emmerling, *Chem. Commun.* **2017**, *53*, 1664–1667.

52 A. Khawam, D. R. Flanagan, *J. Phys. Chem. B* **2006**, *110*, 17315–17328.

53 M. Avrami, *J. Chem. Phys.* **1939**, *7*, 1103–1112.

54 M. Avrami, *J. Chem. Phys.* **1940**, *8*, 212–224.

55 E. G. Prout, F. C. Tompkins, *Trans. Faraday Soc.* **1944**, *40*, 488–498.

56 M. E. Brown, *Thermochim.Acta* **1997**, *300*, 93 – 106.

57 T. Friščić, S. L. Childs, S. A. A. Rizvi, W. Jones, *CrystEngComm* **2009**, *11*, 418–426.

58 A. M. Belenguer, G. I. Lampronti, D. J. Wales, J. K. M. Sanders, *J.Am. Chem. Soc.* **2014**, *136*, 16156–16166.

59 A. Jayasankar, A. Somwangthanaroj, Z. J. Shao, N. Rodríguez-Hornedo, *Pharmaceut. Res.* **2006**, *23*, 2381–2392.